Journal of Fluids and Structures 17 (2003) 813–832

JOURNAL OF FLUIDS AND STRUCTURES

www.elsevier.nl/locate/jnlabr/yjfls

An improved linear model for rotors subject to dissipative annular flows

M. Moreira[a,1], J. Antunes[b,*], H. Pina[c]

[a] *Escola Superior de Tecnologia—Dep. Matemática, Instituto Politécnico de Setúbal, 2914-508 Setúbal, Portugal*
[b] *Applied Dynamics Laboratory, Instituto Tecnológico e Nuclear, 2686-953 Sacavém, Portugal*
[c] *Departamento de Engenharia Mecânica, Instituto Superior Técnico, 1049-001 Lisboa, Portugal*

Received 22 September 2000; accepted 4 October 2002

Abstract

In a previous paper, Antunes, Axisa, and co-workers, developed a linearized model for the dynamic of rotors under moderate fluid confinement, based on classical perturbation analysis, covering two different cases: (i) dissipative motions of a centered rotor; (ii) motions of an eccentric rotor for frictionless flow. Following the same procedures and assumptions, we derive here an improved model for the more general case of *dissipative linearized motions of an eccentric rotor*. Besides the rotor motion variables, a new variable—which can be interpreted as the fluctuating term of the average tangential velocity—is introduced, yielding an additional eigenvalue in the linear analysis. The new variable introduced, which is coupled with the rotor motions, is very convenient when frictional effects are not neglected. Under dissipative flows, a richer modal behavior is highlighted, which can be related to delay effects of the flow responses to the rotor motions. Our approach can be applied as well to other flow-excited systems, for example, those subjected to axial or leakage flows. Because rotor-dynamics are strongly dependent on the mean rotor eccentricity, the adequacy of this (or any other) model rely on using the actual value for such parameter.

1. Introduction

In a previous paper, Antunes et al. (1996), developed a linearized model for the dynamic of rotors under moderate fluid confinement, based on classical perturbation analysis. These authors presented exact analytical results covering two different cases:

1. dissipative linearized motions of a centered rotor;
2. linearized motions of an eccentric rotor for frictionless flows.

Their work showed, in particular, that rotor dynamics are quite sensitive to eccentricity and dissipative effects. Indeed, for moderate or high values of the rotor eccentricity, the system became linearly unstable by divergence—at spinning velocities much lower than those for which concentric rotors flutter. Quantitative differences in the stability boundaries are mostly controlled by the friction-dependent flow terms.

*Corresponding author. Tel.: +351-219-941-039; fax: +351-219-941-039.
E-mail address: jantunes@itn.pt (J. Antunes).
[1] Visiting researcher at ITN/ADL.

0889-9746/03/$ - see front matter © 2003 Published by Elsevier Science Ltd.
doi:10.1016/S0889-9746(03)00023-9

Following the same procedures and assumptions of Antunes et al. (1996), we derive here an improved model to cover the more general case of a *dissipative linearized motion of an eccentric rotor*, for which an exact theoretical analysis presents some further difficulties because the flow-coupling matrices now depend on the motion frequency.

In this general case, which was only previously covered in a coarse manner, the coupling between an auxiliary flow variable and the rotor motions is introduced, yielding an additional eigenvalue in the linear analysis. Numerical results for the modal behavior of the flow-coupled system are then obtained in a straightforward manner, as iterative computations can be avoided.

Under dissipative flows, computations using the present model uncover intricacies in the system modal behavior, which are not displayed by the conservative case.

2. Flow formulation

Consider the geometry of the fluid annulus represented in Fig. 1, where θ and t are, respectively, the azimuth and time, R is the shaft radius and $u(\theta, t)$ is the gap-averaged tangential flow velocity. The annular gap depth $h(\theta, t)$ is very well approximated by

$$h(\theta, t) = H - (X_0 + X(t))\cos\theta - Y(t)\sin\theta, \tag{1}$$

where H is the average annular gap and X_0 is some initial static eccentricity. Note that one can always choose an adequate orientation of coordinate axis to express the initial static eccentricity by X_0.

As in Antunes et al. (1996) the following simplifying assumptions will be adopted concerning the flow field:

1. the flow is modelled as being two-dimensional and incompressible;
2. the radial gradients in the velocity and pressure fields are neglected;
3. the dissipative effects due to turbulent shear stresses at the walls are modelled using semiempirical loss-of-head terms.

Given the above assumptions one can obtain the continuity equation for incompressible flow and the momentum equation (projected in the tangential direction),

$$\frac{\partial h}{\partial t} + \frac{1}{R}\frac{\partial (hu)}{\partial \theta} = 0, \tag{2}$$

$$\rho\left\{\frac{\partial (hu)}{\partial t} + \frac{1}{R}\frac{\partial (hu^2)}{\partial \theta}\right\} + \tau_s + \tau_r + \frac{h}{R}\frac{\partial p}{\partial \theta} = 0, \tag{3}$$

where ρ is the fluid density and $p(\theta, t)$ is the gap-averaged pressure.

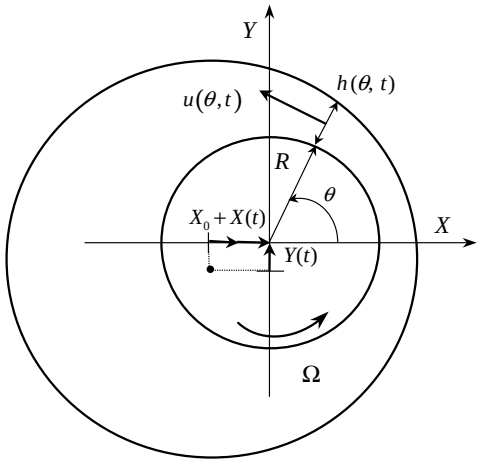

Fig. 1. Geometry of the fluid annulus.

The shear stresses at the rotor and stator walls, in Eq. (3), are given by

$$\tau_s(\theta,t) = \tfrac{1}{2}\rho u|u|f_s,$$

$$\tau_r(\theta,t) = -\tfrac{1}{2}\rho(\Omega R-u)|\Omega R-u|f_r, \tag{4}$$

where f_r and f_s are empirical friction coefficients, which depend on the flow Reynolds number and on wall roughness.

Assuming $f_r = f_s = f$, for the sake of formal simplicity, and adopting also the simplifications discussed in Antunes et al. (1999), we can deduce

$$\tau_s + \tau_r \simeq \rho f \Omega R u - \tfrac{1}{2}\rho f \Omega^2 R^2. \tag{5}$$

Using classical perturbation analysis Eqs. (2) and (3) can be solved, for a given motion of the rotor, by separating the displacement $h(\theta,t)$, the tangential flow velocity $u(\theta,t)$, and the pressure field $p(\theta,t)$, into a steady term, depending on the rotor-average eccentricity, and a small fluctuating term, dependent on the rotor vibratory motion

$$h(\theta,t) = h_0(\theta) + h_1(\theta,t), \tag{6}$$

$$u(\theta,t) = u_0(\theta) + u_1(\theta,t), \tag{7}$$

$$p(\theta,t) = p_0(\theta) + p_1(\theta,t). \tag{8}$$

Let us replace $h(\theta,t)$, $u(\theta,t)$ and $p(\theta,t)$ in Eqs. (2), (3) and (5), by Eqs. (6), (7) and (8). Then, neglecting higher-order products of the fluctuating terms, two sets of differential equations are obtained: (i) zero-order nonlinear flow equations, describing the steady flow field; (ii) first-order linearized equations, describing the fluctuating flow, which apply to small vibratory motions about the static position. These are,

$$\frac{\mathrm{d}}{\mathrm{d}\theta}(h_0 u_0) = 0, \tag{9}$$

$$\frac{\mathrm{d}p_0}{\mathrm{d}\theta} + \rho\frac{u_0^2}{h_0}\frac{\mathrm{d}h_0}{\mathrm{d}\theta} + 2\rho u_0\frac{\mathrm{d}u_0}{\mathrm{d}\theta} + \frac{R\rho}{2h_0}\left[2f\Omega R u_0 - f\Omega^2 R^2\right] = 0 \tag{10}$$

and

$$\frac{\partial h_1}{\partial t} + \frac{1}{R}\frac{\partial}{\partial\theta}(h_0 u_1 + u_0 h_1) = 0, \tag{11}$$

$$\frac{\partial p_1}{\partial\theta} + \frac{1}{h_0}\frac{\mathrm{d}p_0}{\mathrm{d}\theta}h_1 + R\rho\frac{u_0}{h_0}\frac{\partial h_1}{\partial t} + R\rho\frac{\partial u_1}{\partial t} + 2\rho\frac{u_0}{h_0}\frac{\mathrm{d}h_0}{\mathrm{d}\theta}u_1 + \rho\frac{u_0^2}{h_0}\frac{\partial h_1}{\partial\theta} + 2\rho\frac{\mathrm{d}u_0}{\mathrm{d}\theta}u_1 + 2\rho\frac{u_0}{h_0}\frac{\mathrm{d}u_0}{\mathrm{d}\theta}h_1 + 2\rho u_0\frac{\partial u_1}{\partial\theta} + \rho f\Omega R^2\frac{u_1}{h_0} = 0. \tag{12}$$

Eqs. (9)–(12), deduced by the same procedures, can be found in Antunes et al. (1996).

In the following we will be interested, in particular, in the fluctuating form of the dynamic flow forces

$$\frac{F_X(t)}{L} = -R\int_0^{2\pi} p_1(\theta,t)\cos\theta\,\mathrm{d}\theta,$$

$$\frac{F_Y(t)}{L} = -R\int_0^{2\pi} p_1(\theta,t)\sin\theta\,\mathrm{d}\theta, \tag{13}$$

where L is the immersed length of the rotor. Equivalently, integration by parts of Eq. (13) lead to the more convenient form

$$\frac{F_X(t)}{L} = R\int_0^{2\pi}\frac{\partial p_1(\theta,t)}{\partial\theta}\sin\theta\,\mathrm{d}\theta,$$

$$\frac{F_Y(t)}{L} = -R\int_0^{2\pi}\frac{\partial p_1(\theta,t)}{\partial\theta}\cos\theta\,\mathrm{d}\theta. \tag{14}$$

3. Solution of the flow equations

3.1. Analysis of the steady flow

Let the static gap be approximated by

$$h_0(\theta) \approx H(1 - \varepsilon \cos\theta), \tag{15}$$

where $\varepsilon = X_0/H$ is the reduced initial static eccentricity. Then, as in Antunes et al. (1996), from the zero-order flow equations (9) and (10) one can obtain the following steady parameters, which will be needed later to describe the fluctuating flow:

$$u_0(\theta) = K\Omega R \frac{1}{1 - \varepsilon \cos\theta} \tag{16}$$

with $K = \frac{1}{2}(1 - \varepsilon^2)$ and finally,

$$\frac{\partial p_0(\theta)}{\partial \theta} = (\Omega R)^2 \rho \left\{ A_1 \frac{\partial F_2^{00}(\varepsilon, \theta)}{\partial \theta} + A_2 \frac{\partial F_2^{10}(\varepsilon, \theta)}{\partial \theta} + A_3 \frac{\partial F_2^{11}(\varepsilon, \theta)}{\partial \theta} \right\}. \tag{17}$$

In the last equation,

$$A_0 = \tfrac{1}{2} K^2, \tag{18}$$

$$A_1 = -\tfrac{1}{2} K^2, \tag{19}$$

$$A_2 = -Kf\varepsilon \frac{1}{(1 - \varepsilon^2)\delta}, \tag{20}$$

$$A_3 = K\varepsilon^2 f \frac{1}{(1 - \varepsilon^2)\delta} = -A_2\varepsilon, \tag{21}$$

with $\delta = \frac{H}{R}$ and

$$F_k^{ij}(\varepsilon, \theta) = \frac{(\sin\theta)^i (\cos\theta)^j}{(1 - \varepsilon \cos\theta)^k}. \tag{22}$$

3.2. Analysis of the fluctuating flow

From the fluctuating gap

$$h_1 = -X \cos\theta - Y \sin\theta \tag{23}$$

and using Eqs. (15) and (16) one can solve Eq. (11) in order to obtain the fluctuating velocity field

$$u_1(\theta, t) = \frac{K\Omega}{\delta} \frac{\cos\theta}{(1 - \varepsilon \cos\theta)^2} X + \frac{K\Omega}{\delta} \frac{\sin\theta}{(1 - \varepsilon \cos\theta)^2} Y + \frac{1}{\delta} \frac{\sin\theta}{(1 - \varepsilon \cos\theta)} \dot{X} - \frac{1}{\delta} \frac{\cos\theta}{(1 - \varepsilon \cos\theta)} \dot{Y} + \frac{C(t)}{(1 - \varepsilon \cos\theta)}, \tag{24}$$

where $C(t)$ is an integration "constant" related to the co-rotating flow.

Then $h_1(\theta, t)$ and $u_1(\theta, t)$ can be replaced in the momentum equation (12) from which the fluctuating pressure field can be obtained.

Note that Eqs. (23)–(24) can be found as well in Antunes et al. (1996). However, due to a misprint, the fourth term of Eq. (34) in Antunes et al. (1996) has a wrong sign, which was corrected here. Such misprint does not affect the formulation following Eq. (34), in Antunes et al. (1996).

3.3. Resultant fluctuating fluid forces

Considering Eq. (10), and with the knowledge of Eqs. (15)–(17), (23) and, (24), one can deduce by integration,

$$\begin{aligned} f_X &\equiv \frac{F_X(t)}{L} = -R \int_0^{2\pi} \frac{\partial p_1(\theta, t)}{\partial \theta} \sin\theta \, \mathrm{d}\theta \\ &= \mathbb{M}_{XX} \ddot{X} + \mathbb{C}_{XX} \dot{X} + \mathbb{C}_{XY} \dot{Y} + \mathbb{K}_{XX} X + \mathbb{K}_{XY} Y + \mathbb{K}_{XC} C, \end{aligned} \tag{25}$$

$$f_Y \equiv \frac{F_Y(t)}{L} = R\int_0^{2\pi} \frac{\partial p_1(\theta,t)}{\partial\theta}\cos\theta\,\mathrm{d}\theta$$
$$= \mathbb{M}_{YY}\ddot{Y} + \mathbb{C}_{YX}\dot{X} + \mathbb{C}_{YY}\dot{Y} + \mathbb{C}_{YC}\dot{C} + \mathbb{K}_{YX}X + \mathbb{K}_{YY}Y + \mathbb{K}_{YC}C, \tag{26}$$

$$f_C \equiv R\int_0^{2\pi} \frac{\partial p_1(\theta,t)}{\partial\theta}\,\mathrm{d}\theta = 0$$
$$= \mathbb{M}_{CY}\ddot{Y} + \mathbb{C}_{CX}\dot{X} + \mathbb{C}_{CY}\dot{Y} + \mathbb{C}_{CC}\dot{C} + \mathbb{K}_{CX}X + \mathbb{K}_{CY}Y + \mathbb{K}_{CC}C \tag{27}$$

$$= \mathbb{M}_{CY}\ddot{Y} + \mathbb{C}_{CX}\dot{X} + \mathbb{C}_{CY}\dot{Y} + \mathbb{C}_{CC}\dot{C} + \mathbb{K}_{CX}X + \mathbb{K}_{CC}C. \tag{28}$$

Note that, because $\mathbb{K}_{CY} \equiv 0$, one can obtain Eq. (28) from Eq. (27). Eqs. (25) and (26) represent the fluidelastic forces per unit length and Eq. (28) express the continuity of the pressure field.

The inertial, velocity and displacement coupling factors are presented in Appendix A as a function of the integrals

$$G_k^{ij}(\varepsilon) = \int_0^{2\pi} \frac{(\sin\theta)^i(\cos\theta)^j}{(1-\varepsilon\cos\theta)^k}\,\mathrm{d}\theta, \tag{29}$$

which are tabled in Appendix B.

Observe that the dynamics of the system depends on $X(t)$, $Y(t)$ and $C(t)$. This explains why we need three differential equations (25), (26) and (28) to characterize f_X and f_Y which are the focus of our interest. However, in two particular cases (see, Antunes et al., 1996) it is possible to characterize f_X and f_Y with only two equations: (i) dissipative linearized motions of a centered rotor; (ii) linearized motions of an eccentric rotor for a frictionless flow. In these particular situations one can eliminate references to the variable $C(t)$ and its derivative in Eqs. (25) and (26). Indeed the differential equation (28) simplifies for a centered rotor or for a frictionless flow, allowing an explicit solution for $C(t)$.

3.4. Physical meaning of $C(t)$

Integrating each side of the linearized form of the flow rate

$$Q(t) = h_0(\theta)u_0(\theta) + h_1(\theta,t)u_0(\theta) + h_0(\theta)u_1(\theta,t) \tag{30}$$

in $[0, 2\pi]$, one obtains

$$Q(t) = HK\Omega R + HC(t),$$

that is,

$$\bar{u}(t) = C_0 + C(t),$$

where $\bar{u}(t) = Q(t)/H$ is the average tangential flow velocity and $C_0 = K\Omega R$ is the correspondent zero order term. Clearly, $C(t)$ is the first-order fluctuating term of the average tangential flow velocity.

4. Analysis of the coupled system

4.1. Proposed formulation

Let f_X^{st} and f_Y^{st} be the structural dynamic forces per unit shaft length,

$$f_X^{st} = M^{st}\ddot{X} + C^{st}\dot{X} + K^{st}X, \tag{31}$$

$$f_Y^{st} = M^{st}\ddot{Y} + C^{st}\dot{Y} + K^{st}Y, \tag{32}$$

where and M^{st}, C^{st} and K^{st} stand, respectively, for the rigid rotor mass, the damping coefficient and the stiffness of the flexible isotropic rotor fixture. These coefficients are defined per unit length of the rotor. The study of the interaction phenomena induced by the co-rotating flow can be made considering the following complete set of rotordynamic equations:

$$0 = f_X + f_X^{st} = (\mathbb{M}_{XX} + M^{st})\ddot{X} + (\mathbb{C}_{XX} + C^{st})\dot{X} + \mathbb{C}_{XY}\dot{Y} + (\mathbb{K}_{XX} + K^{st})X + \mathbb{K}_{XY}Y + \mathbb{K}_{XC}C, \tag{33}$$

$$0 = f_Y + f_Y^{st} = (\mathbb{M}_{YY} + M^{st})\ddot{Y} + \mathbb{C}_{YX}\dot{X} + (\mathbb{C}_{YY} + C^{st})\dot{Y} + \mathbb{C}_{YC}\dot{C} + \mathbb{K}_{YX}X + (\mathbb{K}_{YY} + K^{st})Y + \mathbb{K}_{YC}C, \tag{34}$$

$$0 = \mathbb{M}_{CY}\ddot{Y} + \mathbb{C}_{CX}\dot{X} + \mathbb{C}_{CY}\dot{Y} + \mathbb{C}_{CC}\dot{C} + \mathbb{K}_{CX}X + \mathbb{K}_{CC}C. \tag{35}$$

Letting $Z = \dot{X}$ and $W = \dot{Y}$ one can study the modal behavior of the system as a function of ε and Ω, by solving the complex eigenvalue $\lambda_n = \sigma_n + \mathrm{i}\nu_n$ and complex eigenvector $\{\Phi_n\}$ problem of the equivalent set of five first-order differential equations:

$$\begin{bmatrix} 1 & 0 & 0 & 0 & 0 \\ 0 & 1 & 0 & 0 & 0 \\ \mathbb{C}_{XX}+C^{st} & \mathbb{C}_{XY} & \mathbb{M}_{XX}+M^{st} & 0 & 0 \\ \mathbb{C}_{YX} & \mathbb{C}_{YY}+C^{st} & 0 & \mathbb{M}_{YY}+M^{st} & \mathbb{C}_{YC} \\ \mathbb{C}_{CX} & \mathbb{C}_{CY} & 0 & \mathbb{M}_{CY} & \mathbb{C}_{CC} \end{bmatrix} \begin{bmatrix} \dot{X} \\ \dot{Y} \\ \dot{Z} \\ \dot{W} \\ \dot{C} \end{bmatrix} + \begin{bmatrix} 0 & 0 & -1 & 0 & 0 \\ 0 & 0 & 0 & -1 & 0 \\ \mathbb{K}_{XX}+K^{st} & \mathbb{K}_{XY} & 0 & 0 & \mathbb{K}_{XC} \\ \mathbb{K}_{YX} & \mathbb{K}_{YY}+K^{st} & 0 & 0 & \mathbb{K}_{YC} \\ \mathbb{K}_{CX} & 0 & 0 & 0 & \mathbb{K}_{CC} \end{bmatrix} \begin{bmatrix} X \\ Y \\ Z \\ W \\ C \end{bmatrix} = \begin{bmatrix} 0 \\ 0 \\ 0 \\ 0 \\ 0 \end{bmatrix}. \tag{36}$$

From each eigenvalue $\lambda_n = \sigma_n + \mathrm{i}\nu_n$ the corresponding reduced modal frequency and reduced modal damping can be computed as

$$\varpi_n = \frac{\nu_n}{\omega^{st}},$$

$$\overline{d}_n = \frac{-\sigma_n}{\omega^{st}},$$

where ω^{st} is the structural circular frequency in vacuum.

Note that 0, 1 or 2 complex conjugate pairs of eigenvalues (and eigenvectors) would be expected in the complete set of 5 eigenvalues (and eigenvectors) of the problem. One of these eigenvalues must be always real. Note that the coupling matrices depend on Ω and ε but are otherwise constant.

4.2. Alternative formulation

Note that in the precedent analysis we deal with a new variable, $C(t)$. However, if one is only interested in an eigenvalue analysis, by assuming a solution in the form

$$\overline{S} = \begin{bmatrix} \tilde{X} \\ \tilde{Y} \\ \tilde{C} \end{bmatrix} \mathrm{e}^{\lambda t},$$

and replacing it in Eqs. (33), (34) and (35) one can deduce after eliminating $\tilde{C}$

$$\{\lambda^2\mathbb{M}(\lambda) + \lambda\mathbb{C}(\lambda) + \mathbb{K}(\lambda)\} \begin{bmatrix} \tilde{X} \\ \tilde{Y} \end{bmatrix} = \begin{bmatrix} 0 \\ 0 \end{bmatrix}, \tag{37}$$

where

$$\mathbb{M}(\lambda) = \begin{bmatrix} (\mathbb{M}_{XX}+M^{st}) & \dfrac{\mathbb{M}_{CY}\mathbb{K}_{XC}}{(\lambda\mathbb{C}_{CC}+\mathbb{K}_{CC})} \\ \dfrac{-\mathbb{C}_{YC}\mathbb{C}_{CX}}{(\lambda\mathbb{C}_{CC}+\mathbb{K}_{CC})} & (\mathbb{M}_{YY}+M^{st}) - \dfrac{\mathbb{K}_{YC}\mathbb{M}_{CY}+\mathbb{C}_{YC}\mathbb{C}_{CY}}{(\lambda\mathbb{C}_{CC}+\mathbb{K}_{CC})} - \lambda\dfrac{\mathbb{C}_{YC}\mathbb{M}_{CY}}{(\lambda\mathbb{C}_{CC}+\mathbb{K}_{CC})} \end{bmatrix},$$

$$\mathbb{C}(\lambda) = \begin{bmatrix} (\mathbb{C}_{XX}+C^{st}) - \dfrac{\mathbb{C}_{CX}\mathbb{K}_{XC}}{(\lambda\mathbb{C}_{CC}+\mathbb{K}_{CC})} & \mathbb{C}_{XY} - \dfrac{\mathbb{C}_{CY}\mathbb{K}_{XC}}{(\lambda\mathbb{C}_{CC}+\mathbb{K}_{CC})} \\ \mathbb{C}_{YX} - \dfrac{\mathbb{K}_{YC}\mathbb{C}_{CX}+\mathbb{C}_{YC}\mathbb{K}_{CX}}{(\lambda\mathbb{C}_{CC}+\mathbb{K}_{CC})} & (\mathbb{C}_{YY}+C^{st}) - \dfrac{\mathbb{K}_{YC}\mathbb{C}_{CY}}{(\lambda\mathbb{C}_{CC}+\mathbb{K}_{CC})} \end{bmatrix},$$

$$\mathbb{K}(\lambda) = \begin{bmatrix} (\mathbb{K}_{XX}+K^{st}) - \dfrac{\mathbb{K}_{CX}\mathbb{K}_{XC}}{(\lambda\mathbb{C}_{CC}+\mathbb{K}_{CC})} & \mathbb{K}_{XY} \\ \mathbb{K}_{YX} - \dfrac{\mathbb{K}_{YC}\mathbb{K}_{CX}}{(\lambda\mathbb{C}_{CC}+\mathbb{K}_{CC})} & (\mathbb{K}_{YY}+K^{st}) \end{bmatrix}.$$

Observe that all the three matrices obtained, $\mathbb{M}$, $\mathbb{C}$ and $\mathbb{K}$, are now depend on the eigenvalues λ. In other words, they depend on the motion frequency and the eigenvalue problem becomes therefore nonlinear. Thus, to solve the new generalized eigenvalue problem (37), and find the modal properties of the system, it is necessary to apply an iterative

method for each and every eigenvalue. This type of formulation, which is often found in literature, is obviously somewhat awkward.

As a matter of fact, if the flow is nondissipative ($f = 0$), the matrices in Eq. (37) will simplify so that they do not depend on λ. In this case one can deduce

$$\{\lambda^2\mathbb{N}_1 + \lambda\mathbb{N}_2 + \mathbb{N}_3\}\begin{bmatrix}\tilde{X}\\ \tilde{Y}\end{bmatrix} = \begin{bmatrix}0\\ 0\end{bmatrix}, \tag{38}$$

where

$$\mathbb{N}_1 = \begin{bmatrix}(M^{st} + \mathbb{M}_{XX}) & 0\\ 0 & (M^{st} + \mathbb{M}_{YY}) - \dfrac{\mathbb{C}_{YC}\mathbb{M}_{CY}}{\mathbb{C}_{CC}}\end{bmatrix}$$

$$= \begin{bmatrix}M^{st} + \dfrac{\pi\rho R^2}{\delta}\dfrac{2(1-\sqrt{1-\varepsilon^2})}{\varepsilon^2} & 0\\ 0 & M^{st} + \dfrac{\pi\rho R^2}{\delta}\dfrac{2(1-\sqrt{1-\varepsilon^2})}{\varepsilon^2}\end{bmatrix},$$

$$\mathbb{N}_2 = \begin{bmatrix}C^{st} & \mathbb{C}_{XY} - \dfrac{\mathbb{M}_{CY}\mathbb{K}_{XC}}{\mathbb{C}_{CC}}\\ \mathbb{C}_{YX} - \dfrac{\mathbb{C}_{YC}\mathbb{C}_{CX}}{\mathbb{C}_{CC}} & C^{st}\end{bmatrix}$$

$$= \begin{bmatrix}C^{st} & \dfrac{\pi\rho R^2}{\delta}\Omega\\ -\dfrac{\pi\rho R^2}{\delta}\Omega & C^{st}\end{bmatrix}$$

and

$$\mathbb{N}_3 = \begin{bmatrix}(K^{st} + \mathbb{K}_{XX}) - \dfrac{\mathbb{C}_{CX}\mathbb{K}_{XC}}{\mathbb{C}_{CC}} & 0\\ 0 & (K^{st} + \mathbb{K}_{YY})\end{bmatrix}$$

$$= \begin{bmatrix}K^{st} - \dfrac{\pi\rho R^2}{\delta}\dfrac{\Omega^2}{4}\dfrac{1}{\sqrt{(1-\varepsilon^2)}} & 0\\ 0 & K^{st} - \dfrac{\pi\rho R^2}{\delta}\dfrac{\Omega^2}{4}\sqrt{(1-\varepsilon^2)}\end{bmatrix}.$$

Note that the coupling coefficients related to the fluctuating fluid forces, in matrices $\mathbb{N}_1$, $\mathbb{N}_2$ and $\mathbb{N}_3$, are precisely the same obtained by Antunes et al. (1996) when describing the formulation of the fluid forces as a function of the eccentricity ε, if dissipative effects are neglected.

The dependence of the coupling matrices on the motion frequency can be interpreted as a time-delay in the flow response to the rotor vibrations. To show that the flow response of the dissipative system is delayed with respect to rotor motions we will briefly study the simpler planar case. Letting $Y = \dot{Y} = \ddot{Y} = 0$, Eq. (35) collapse into the differential equation

$$\mathbb{C}_{CX}\dot{X} + \mathbb{C}_{CC}\dot{C} + \mathbb{K}_{CX}X + \mathbb{K}_{CC}C = 0 \tag{39}$$

which relates the flow response and the rotor motion. That is,

$$C(t) = -\mathrm{e}^{-(\mathbb{K}_{CC}/\mathbb{C}_{CC})t}\int \mathrm{e}^{(\mathbb{K}_{CC}/\mathbb{C}_{CC})t}\left(\frac{\mathbb{C}_{CX}\dot{X} + \mathbb{K}_{CX}X}{\mathbb{C}_{CC}}\right)\mathrm{d}t. \tag{40}$$

Assuming harmonic rotor motions

$$X(t) = \tilde{X}\mathrm{e}^{\lambda t}, \tag{41}$$

where λ is a complex number, we obtain

$$C(t) = -\frac{\mathbb{K}_{CX} + \lambda\mathbb{C}_{CX}}{\mathbb{K}_{CC} + \lambda\mathbb{C}_{CC}}\tilde{X}\mathrm{e}^{\lambda t}. \tag{42}$$

So, one can identify a phase delay $\phi(\lambda)$ between (41) and (42) which can be computed as

$$\phi(\lambda) = \arg\left(\frac{C(t)}{X(t)}\right)$$

or

$$\phi(\lambda) = \arg\left(-\frac{\mathbb{K}_{CX} + \lambda\mathbb{C}_{CX}}{\mathbb{K}_{CC} + \lambda\mathbb{C}_{CC}}\right).$$

Observe that if $f = 0$, then $\mathbb{K}_{CX} = \mathbb{K}_{CC} = 0$ and

$$\phi = \arg\left(-\frac{\mathbb{C}_{CX}}{\mathbb{C}_{CC}}\right) \equiv 0,$$

that is, the response delay of a nondissipative bulk-flow is zero.

One can additionally note that if $\varepsilon = 0$ then $\mathbb{C}_{CX} = \mathbb{K}_{CX} = 0$. This case yields also a zero delay between the flow response and the rotor motion, for both dissipative and nondissipative flows:

$$\phi = \arg\left(-\frac{0}{\mathbb{K}_{CC} + \lambda\mathbb{C}_{CC}}\right) \equiv 0.$$

Similar time-delay effects were noted by Porcher (1994), when addressing structures subjected to confined axial flows.

In fact this kind of effect is also common in the field of viscous flow over compliant boundaries (see, for instance, Carpenter and Garrad, 1986).

5. Numerical computations

As mentioned before concerning the eigenvalue analysis of system (36), it is expectable to find 0, 1 or 2 complex conjugate pairs of eigenvalues (and eigenvectors) for this problem. This means that 5, 3 or 1, of the complete set of 5 eigenvalues, will be real, respectively. Therefore, numerical results presented here do account for this fact.

Observe that each conjugate pair of complex eigenvalues/eigenvectors corresponds to an oscillatory *mode*. The remaining real eigenvalues/eigenvectors are associated with nonoscillatory motions. The system modes can be represented by the corresponding frequency (imaginary part of the eigenvalue) and damping (real part of the same eigenvalue) values, which depend on the spinning velocity and rotor eccentricity. From the computed eigenvectors, oscillatory modes can be additionally characterized by a well-defined *forward* or *backward whirl*. The computed modes will be identified in the plots using the following codes: F and B, respectively, for the forward and backward whirling modes and Z for zero-frequency modes.

The reduced modal frequencies $\varpi_n = \nu_n/\omega^{st}$ will be shown as a function of the reduced rotor velocity $\overline{\Omega} = \Omega/\omega^{st}$, as well the corresponding damping coefficient $\overline{d}_n = -\sigma_n/\omega^{st}$.

In order to be able to compare the present results with previous work, (Antunes et al. 1996) we have assumed a mass ratio $\gamma = M_a/M_{st} = 2$, a reduced gap of $\delta = H/R = 0.1$ and we have neglected all dissipative structural effects in almost all numerical simulations. The only exception concerns the last computations, presented in paragraph.

5.1. Simple cases accounted for by the previous theory

In Figs. 2–5 we present some particular cases which have in common the fact they concern *dissipative linearized motions of a centered rotor* or *linearized motions of an eccentric rotor for a frictionless flow*. That is, cases which are properly accounted for by the previous linear theory developed by Antunes et al. (1996).

The numerical results presented in Figs. 2–5 display the same forward and backward whirling modes represented in Figs. 11, 12 and 13 of Antunes et al. (1996). Of course, one additional stable eigenvalue (at zero frequency) stems for the present theory, but all other aspects are identical to previous results.

5.2. The dissipative-eccentric case

In Figs. 6–8 the general case of a *dissipative linearized motion of an eccentric rotor* is considered, as a function of the fluid friction parameter f. As it was stressed before, in these computations we have neglected all dissipative structural (nonrotating) effects. However we note that those effects, in our configuration, simply defer the stability boundary as it is common for such systems (see, for instance, Krämer, 1993 or Genta, 1995).

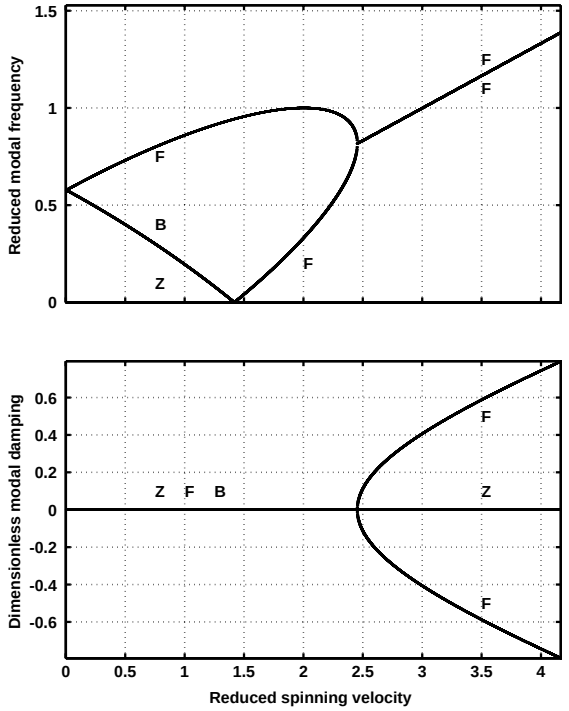

Fig. 2. Rotor modes as a function of the reduced spinning velocity $\overline{\Omega}$ (rotor eccentricity $\varepsilon = 0$; fluid friction neglected; mass ratio $\gamma = 2$).

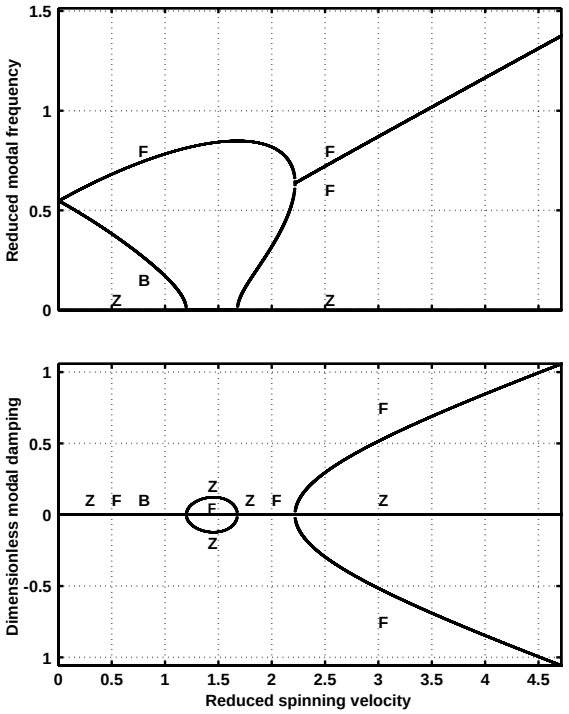

Fig. 3. Rotor modes as a function of the reduced spinning velocity $\overline{\Omega}$ (rotor eccentricity $\varepsilon = 0.7$; fluid friction neglected; mass ratio $\gamma = 2$).

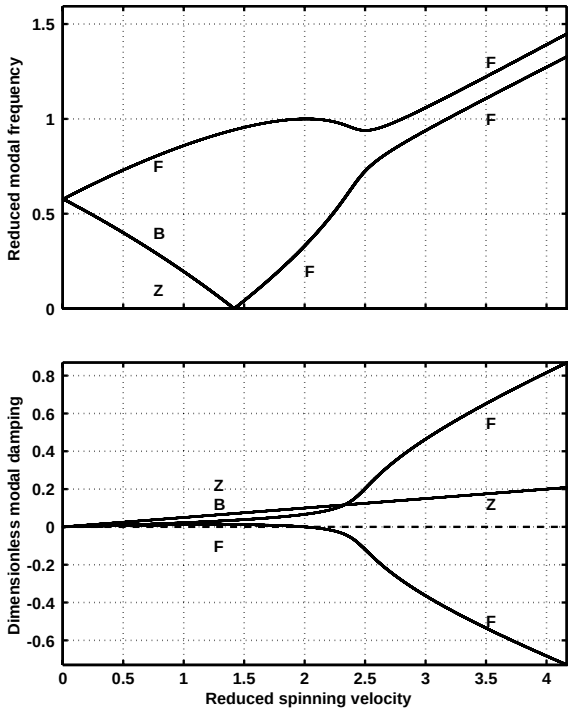

Fig. 4. Rotor modes as a function of the reduced spinning velocity $\overline{\Omega}$ (rotor eccentricity $\varepsilon = 0$; fluid friction $f = 0.005$; mass ratio $\gamma = 2$).

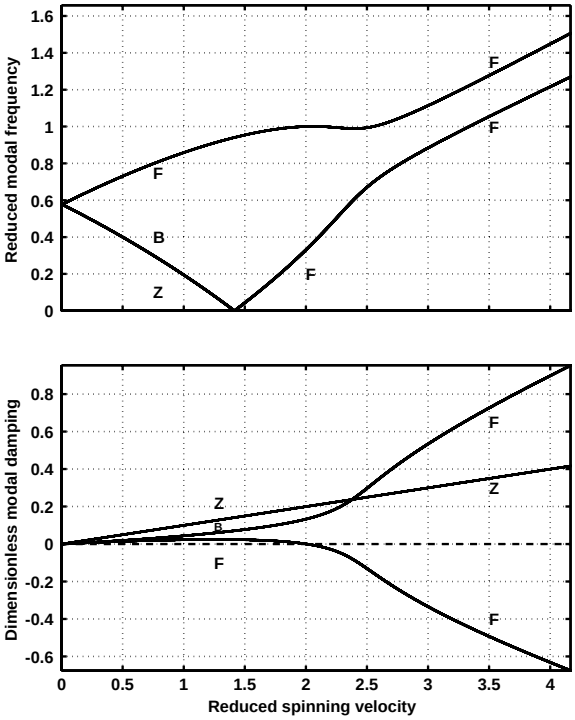

Fig. 5. Rotor modes as a function of the reduced spinning velocity $\overline{\Omega}$ (rotor eccentricity $\varepsilon = 0$; fluid friction $f = 0.01$; mass ratio $\gamma = 2$).

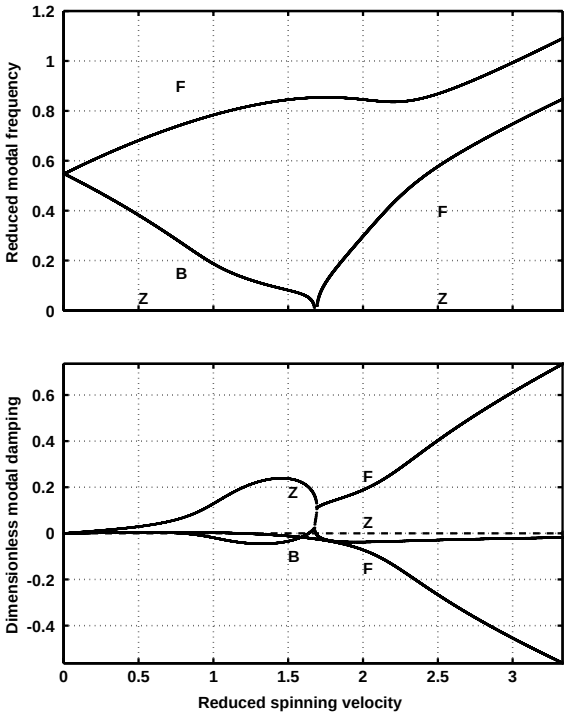

Fig. 6. Rotor modes as a function of the reduced spinning velocity $\overline{\Omega}$ (rotor eccentricity $\varepsilon = 0.7$; fluid friction $f = 0.0025$; mass ratio $\gamma = 2$) (Present formulation).

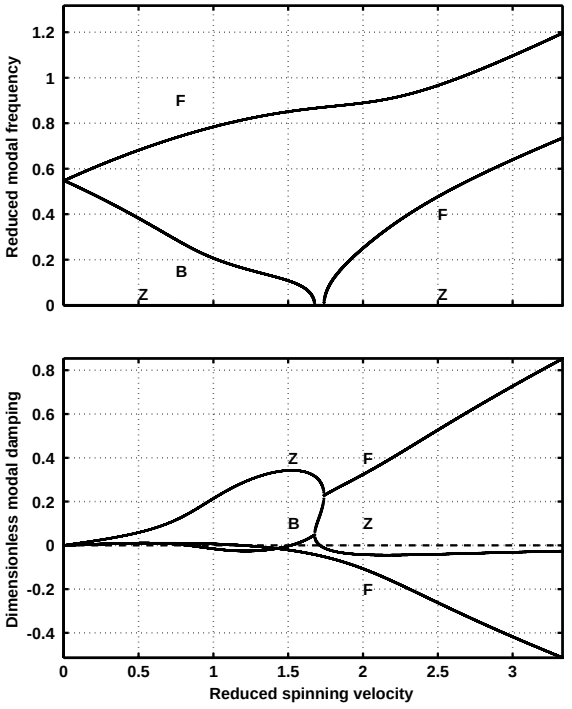

Fig. 7. Rotor modes as a function of the reduced spinning velocity $\overline{\Omega}$ (rotor eccentricity $\varepsilon = 0.7$; fluid friction $f = 0.005$; mass ratio $\gamma = 2$) (Present formulation).

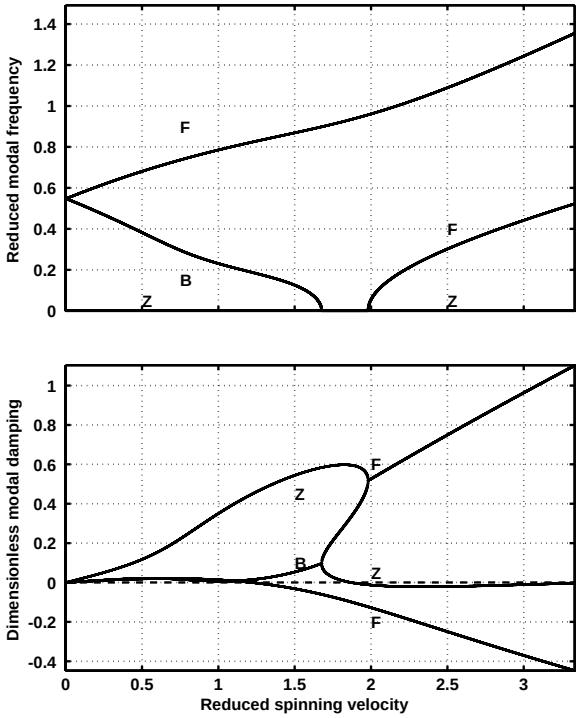

Fig. 8. Rotor modes as a function of the reduced spinning velocity $\overline{\Omega}$ (rotor eccentricity $\varepsilon = 0.7$; fluid friction $f = 0.01$; mass ratio $\gamma = 2$) (Present formulation).

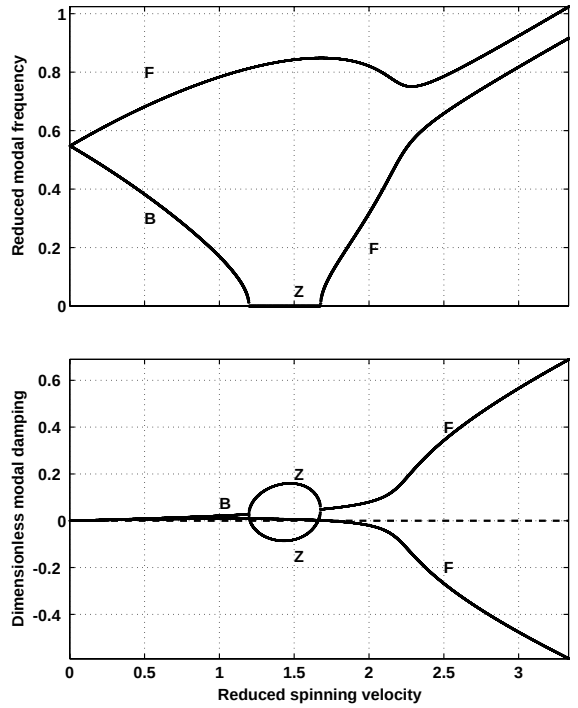

Fig. 9. Rotor modes as a function of the reduced spinning velocity $\overline{\Omega}$ (rotor eccentricity $\varepsilon = 0.7$; fluid friction $f = 0.005$; mass ratio $\gamma = 2$) (Numerical results computed as in Antunes et al., 1996).

The numerical results using the present exact formulation can be quite different from the corresponding results computed as in Antunes et al. (1996). This fact is illustrated, for instance, by comparing Figs. 7 (present formulation) and 9 (computed using the former approach by Antunes et al., 1996). The straightforward but crude approach adopted at that time, for the dynamic analysis of the general case, was simply to combine the conservative coupling terms, stemming from frictionless analysis of the eccentric system, with the dissipative terms stemming from a centered configuration.

Comparing Figs. 7 (present formulation) and 9 (former approach) one can notice that:

- The pattern of modal frequencies $\overline{\omega}_n$, as a function of the spinning velocity $\overline{\Omega}$, is qualitatively similar but displays significant quantitative differences (in particular in the lower values of $\overline{\omega}_n$).
- More important, the relatively simple pattern of the modal damping $\overline{d}_n$ predicted by the crude model has been replaced by a more complex pattern where all the eigenvalues are interlaced.
- The range of $\overline{\Omega}$ where divergence instability was predicted is now much smaller. In practice, for the present test case, the system loses stability by flutter of the backward whirling mode, instead of the divergence predicted earlier.

Observing the reduced modal damping curves displayed in Figs. 6–8, one can notice that, as the internal (rotating, flow-related) damping increases, the stability boundaries are deferred. That is, internal damping is stabilizing for the rotor-flow configuration addressed in this paper. Interestingly we also observed this behavior for other values of M_a/M^{st} and δ.

The matrix representation of the dissipation effects of our centered isotropic rotor can be modelled as follows:

$$\begin{bmatrix} F_X^{\text{dissipative}} \\ F_Y^{\text{dissipative}} \end{bmatrix} = -\begin{bmatrix} C_E + c_I\Omega & 0 \\ 0 & C_E + c_I\Omega \end{bmatrix}\begin{bmatrix} \dot{X} \\ \dot{Y} \end{bmatrix} - \begin{bmatrix} 0 & c_I\dfrac{\Omega^2}{2} \\ -c_I\dfrac{\Omega^2}{2} & 0 \end{bmatrix}\begin{bmatrix} X \\ Y \end{bmatrix},$$

where C_E and $c_I\Omega$ stand, respectively, for the external and internal damping. Note that C_E and the factor c_I are independent of the spinning velocity Ω. An analysis of this system leads to the conclusion that internal damping is associated to dissipative and circulatory terms in the corresponding matrices, and so can exhibit stabilizing as well as destabilizing effects, depending on the spinning velocity Ω. This situation is not very different from the one obtained when formulating the dynamics of the Jeffcott rotor with internal damping, for which rotating damping is stabilizing below the critical velocity and induces instability effects in the supercritical range (see, for instance, Genta, 1995 or Ginsberg, 2001). However, for such basic problem, the dependence of the coupling coefficients on Ω is different from ours. For moderate δ—our case—the rotordynamic model has one additional coupled equation (33) related with the co-rotating flow—$C = C(t)$. This fact leads to a more complex behavior as far as modal damping is concerned and deserves a deeper analysis.

In Moreira et al. (2000a) this improved linear model was applied using Grunenwald et al. (1996) experimental parameters for two different geometries and significant eccentricities, showing that the present improved formulation leads to better predictions. In Moreira et al. (2000b), extensive experimental work has been produced, where the present improved linear model was experimentally validated using a new rotor geometry and several eccentricities. These results stress the relevance of the analytical approach presented here.

5.3. *Using the actual rotor eccentricity*

Numerical computations shown in this section are based on experiments (using water) performed by Grunenwald et al. (1996) and on corresponding numerical simulations using a fully nonlinear model (Moreira et al., 2000a). In such experiments and nonlinear simulations the test case was labelled "eccentric configuration B". The significant parameters used will be repeated here for completeness in Table 1.

As stated before dissipative structural effects will now be also considered in the computations. The modal frequency and damping values will be presented in a nonreduced form.

System dynamics are strongly dependent on the rotor eccentricity. Indeed, a significant drift can be observed as a function of the spinning velocity—see Grunenwald et al. (1996)—which is mostly due to a Bernoulli effect. Moreover, the linearized equations which describe the fluctuating flow only apply to small vibratory motions about the static position of the rotor. These facts motivate the use of the *actual rotor eccentricity* (or, at least, an estimate of it) for the eigenvalue analysis.

In Fig. 10 one can see the computed eigenvalues when using the same static rotor eccentricity (defined at $\Omega = 0$) for every spinning velocity. Fig. 11 shows the corresponding results if the actual rotor eccentricity as a function of Ω (e.g., accounting for the rotor drift) is used when computing the flow-coupling coefficients. In practice, the actual rotor

Table 1
Parameters of simulations to test the influence of the drift

Eccentric configuration	B
L (rotor length (m))	0.250
R (rotor radius (m))	0.0435
H (average annular gap (m))	0.0067
$\delta = \frac{H}{R}$ (reduced gap)	0.154
ε (reduced initial static eccentricity)	0.6
M^{st} (structural mass (kg))	7.0
C^{st} (structural damping (Ns/m))	35
K^{st} (structural stiffness (N/m))	1.6×10^4
f^{st} (structural frequency: $\frac{1}{2\pi}\sqrt{\frac{K_{st}}{M_{st}}}$ (Hz))	7.6

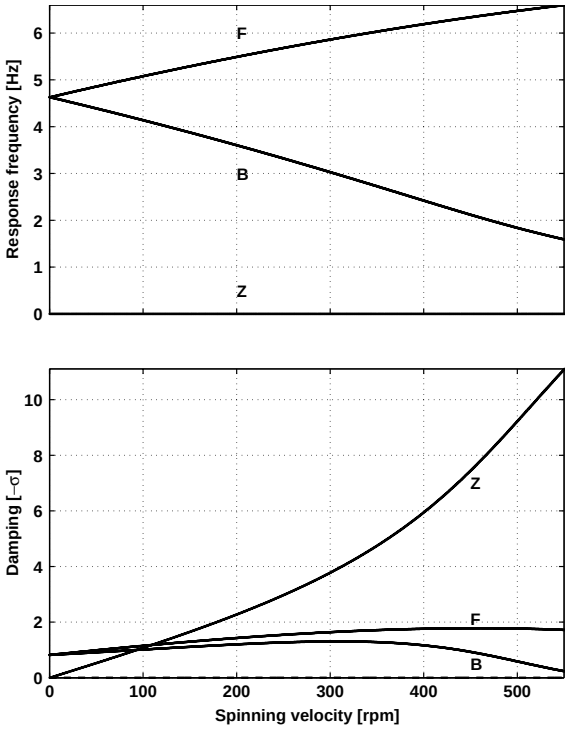

Fig. 10. Rotor modes as a function of the spinning velocity, using the same static eccentricity at every spinning velocity ($\varepsilon = 0.6$, "*eccentric configuration* B" in Grunenwald et al., 1996; Moreira et al., 2000a).

eccentricity were extracted from nonlinear dynamical simulations at several spinning velocities, as shown in Fig. 12 (Moreira et al., 2000a). Then interpolated values were used for the modal computations, as a function of Ω, by fitting a spline to the regularly spaced numerical values.

The differences exhibited by the eigenvalues in Figs. 10 and 11 justify the later approach. An estimate of the rotor drift, as a function of the spinning velocity may be also obtained by an iterative solution of the zero order (static) flow-structure equations (see Antunes et al., 1996).

6. Conclusions

An improved linear model for rotors subjected to dissipative annular flows, based on classical perturbation analysis, was developed in this paper.

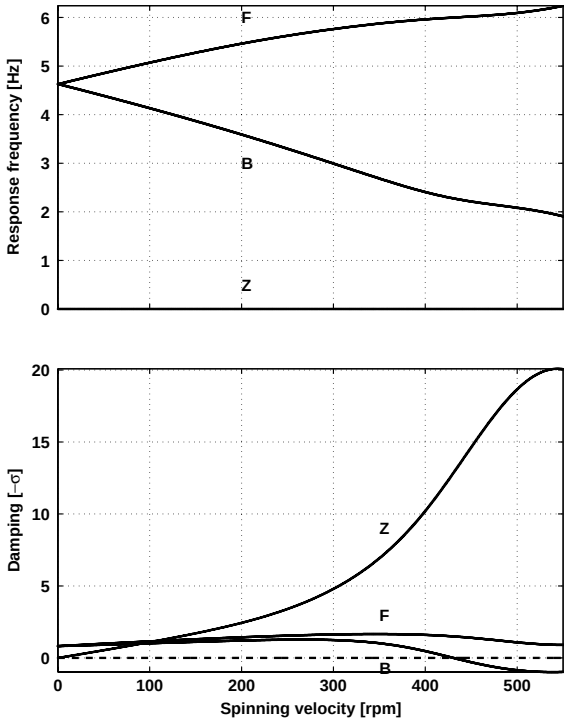

Fig. 11. Rotor modes as a function of the spinning velocity, using the actual eccentricity ("*eccentric configuration* B" in Grunenwald et al., 1996; Moreira et al., 2000a).

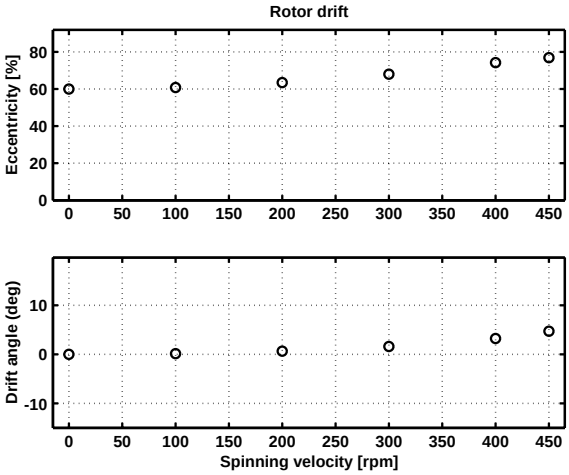

Fig. 12. Rotor drift as a function of the spinning velocity ("*eccentric configuration* B" in Moreira et al., 2000a).

Besides the natural response variables $X(t)$ and $Y(t)$ of the problem, a new flow variable $C(t)$—which can be physically interpreted as the fluctuating term of the average tangential flow velocity—was introduced, yielding an additional eigenvalue in the linear analysis. Whenever boundary pressure values are controlled by dissipative effects, it becomes quite interesting to use this additional flow variable.

We stress that the proposed methodology to avoid frequency-dependent flow-coupling matrices—e.g., using one auxiliary variable and an additional first-order differential equation—can be applied, as well, to different systems. In

vibrating structures subjected to axial flow, our approach was also recently applied with rather satisfactory results (Antunes and Piteau, 2001). In Porcher (2000), Kaneko et al. (2000) and Inada and Hayama (2000) one can find some interesting problems (characterized by axial or leakage flows) for which the usage of this approach might also be beneficial.

The present model is an extension of the theory developed by Antunes et al. (1996). It shows identical predictions in two specific cases, which are exactly accounted for by the previous model, namely: (i) dissipative linearized motions of a centered rotor; (ii) motions of an eccentric rotor for frictionless flow. However, the new approach also yields exact results for the general case of *dissipative motions of eccentric rotors*.

Use of the new variable introduced $C(t)$, coupled with $X(t)$ and $Y(t)$, uncovers a richer modal behavior which incorporates any delay effects of the flow responses to the rotor motions.

As a final note, let us stress that the validity of this (or any other) model is dependent on an adequate estimation of the rotor eccentricity, because system dynamics are strongly dependent on the actual value of this parameter.

Acknowledgements

The authors wish to thank the anonymous reviewers whose contributions significantly improved this paper.

Appendix A. Linear equation factors

A list is given below. In the following equations $K = \frac{1}{2}(1-\varepsilon^2)$

$$\mathbb{M}_{XX} = \frac{\rho R^2}{\delta} G_1^{20}, \tag{A.1}$$

$$\mathbb{C}_{XX} = \frac{\rho R^2}{\delta}\frac{f\Omega}{\delta} G_2^{20}, \tag{A.2}$$

$$\mathbb{C}_{XY} = \frac{\rho R^2}{\delta} 2K\Omega G_3^{20}, \tag{A.3}$$

$$\mathbb{K}_{XX} = \frac{\rho R^2}{\delta}(K\Omega)^2(G_3^{20} - 2G_4^{20} - \varepsilon G_4^{21}), \tag{A.4}$$

$$\mathbb{K}_{XY} = \frac{\rho R^2}{\delta} f\frac{K\Omega^2}{\delta}\left(-\frac{\varepsilon^2}{(1-\varepsilon^2)}(G_4^{20} + G_4^{22}) + \frac{\varepsilon(1+\varepsilon^2)}{(1-\varepsilon^2)} G_4^{21} + G_3^{20}\right), \tag{A.5}$$

$$\mathbb{K}_{XC} = -2\rho K\Omega R^2 \varepsilon G_3^{20}, \tag{A.6}$$

$$\mathbb{M}_{YY} = \frac{\rho R^2}{\delta} G_1^{02}, \tag{A.7}$$

$$\mathbb{C}_{YY} = \frac{\rho R^2}{\delta} f\frac{\Omega}{\delta} G_2^{02}, \tag{A.8}$$

$$\mathbb{C}_{YX} = \frac{\rho R^2}{\delta} 2K\Omega(-G_3^{02} + \varepsilon G_3^{01}), \tag{A.9}$$

$$\mathbb{C}_{YC} = -\rho R^2 G_1^{01}, \tag{A.10}$$

$$\mathbb{K}_{YX} = \frac{\rho R^2}{\delta} f\frac{K\Omega^2}{\delta}\left(\frac{\varepsilon^2}{(1-\varepsilon^2)}(G_4^{02} + G_4^{04}) - \frac{\varepsilon(1+\varepsilon^2)}{(1-\varepsilon^2)} G_4^{03} - G_3^{02}\right), \tag{A.11}$$

$$\mathbb{K}_{YY} = \frac{\rho R^2}{\delta}(K\Omega)^2(G_3^{02} - \varepsilon G_4^{21} - 2G_4^{02} - 2\varepsilon G_4^{03} + 4\varepsilon G_4^{01}), \tag{A.12}$$

$$\mathbb{K}_{YC} = -\frac{\rho R^2}{\delta} f\Omega G_2^{01}, \tag{A.13}$$

$$\mathbb{M}_{CY} = \frac{\rho R^2}{\delta} G_1^{01}, \tag{A.14}$$

$$\mathbb{C}_{CC} = -R^2 \rho G_1^{00}, \tag{A.15}$$

$$\mathbb{C}_{CX} = \frac{\rho R^2}{\delta} 2K\Omega(-G_3^{01} + \varepsilon G_3^{00}), \tag{A.16}$$

$$\mathbb{C}_{CY} = \frac{\rho R^2}{\delta} f \frac{\Omega}{\delta} G_2^{01}, \tag{A.17}$$

$$\mathbb{K}_{CX} = \frac{\rho R^2}{\delta} fK\Omega^2 \left(\frac{\varepsilon^2}{(1-\varepsilon^2)\delta} (G_4^{01} + G_4^{03}) - \frac{\varepsilon(1+\varepsilon^2)}{(1-\varepsilon^2)\delta} G_4^{02} - \frac{1}{\delta} G_3^{01} \right), \tag{A.18}$$

$$\mathbb{K}_{CC} = -\frac{\rho R^2}{\delta} f\Omega G_2^{00}. \tag{A.19}$$

Appendix B. Azimuthal integrals

The azimuthal integrals in Appendix A are given as follows:

$$G_1^{00} = \frac{2\pi}{\sqrt{1-\varepsilon^2}}, \tag{B.1}$$

$$G_1^{01} = \begin{cases} \frac{2\pi\left(1-\sqrt{1-\varepsilon^2}\right)}{\varepsilon\sqrt{1-\varepsilon^2}} & \text{if } 0<\varepsilon<1, \\ 0 & \text{if } \varepsilon = 0, \end{cases} \tag{B.2}$$

$$G_1^{02} = \begin{cases} \frac{2\pi(1-\sqrt{1-\varepsilon^2})}{\varepsilon^2\sqrt{1-\varepsilon^2}} & \text{if } 0<\varepsilon<1, \\ \pi & \text{if } \varepsilon = 0, \end{cases} \tag{B.3}$$

$$G_1^{20} = \begin{cases} \frac{2\pi(1-\sqrt{1-\varepsilon^2})}{\varepsilon^2} & \text{if } 0<\varepsilon<1, \\ \pi & \text{if } \varepsilon = 0, \end{cases} \tag{B.4}$$

$$G_2^{00} = \frac{2\pi}{\sqrt{(1-\varepsilon^2)^3}}, \tag{B.5}$$

$$G_2^{01} = \frac{2\pi\varepsilon}{\sqrt{(1-\varepsilon^2)^3}}, \tag{B.6}$$

$$G_2^{02} = \begin{cases} \frac{2\pi(2\varepsilon^2-1+\sqrt{(1-\varepsilon^2)^3})}{\varepsilon^2\sqrt{(1-\varepsilon^2)^3}} & \text{if } 0<\varepsilon<1, \\ \pi & \text{if } \varepsilon = 0, \end{cases} \tag{B.7}$$

$$G_2^{20} = \begin{cases} \frac{2\pi(1-\sqrt{1-\varepsilon^2})}{\varepsilon^2\sqrt{1-\varepsilon^2}} & \text{if } 0<\varepsilon<1, \\ \pi & \text{if } \varepsilon = 0, \end{cases} \tag{B.8}$$

$$G_3^{00} = \begin{cases} \frac{\pi(\varepsilon^2+2)}{\sqrt{(1-\varepsilon^2)^5}} & \text{if } 0<\varepsilon<1, \\ 2\pi & \text{if } \varepsilon = 0, \end{cases} \tag{B.9}$$

$$G_3^{01} = \begin{cases} \frac{3\pi\varepsilon}{\sqrt{(1-\varepsilon^2)^5}} & \text{if } 0<\varepsilon<1, \\ 0 & \text{if } \varepsilon = 0, \end{cases} \tag{B.10}$$

$$G_3^{02} = \begin{cases} \frac{\pi(2\varepsilon^2+1)}{\sqrt{(1-\varepsilon^2)^5}} & \text{if } 0<\varepsilon<1, \\ \pi & \text{if } \varepsilon = 0, \end{cases} \tag{B.11}$$

$$G_3^{20} = \begin{cases} \frac{\pi}{\sqrt{(1-\varepsilon^2)^3}} & \text{if } 0<\varepsilon<1, \\ \pi & \text{if } \varepsilon = 0, \end{cases} \tag{B.12}$$

$$G_4^{01} = \begin{cases} \frac{\pi\varepsilon(\varepsilon^2+4)}{\sqrt{(1-\varepsilon^2)^7}} & \text{if } 0<\varepsilon<1, \\ 0 & \text{if } \varepsilon = 0, \end{cases} \tag{B.13}$$

$$G_4^{02} = \begin{cases} \frac{\pi(4\varepsilon^2+1)}{\sqrt{(1-\varepsilon^2)^7}} & \text{if } 0<\varepsilon<1, \\ \pi & \text{if } \varepsilon = 0, \end{cases} \tag{B.14}$$

$$G_4^{03} = \begin{cases} \frac{\pi(2\varepsilon^2+3)\varepsilon}{\sqrt{(1-\varepsilon^2)^7}} & \text{if } 0<\varepsilon<1, \\ 0 & \text{if } \varepsilon = 0, \end{cases} \tag{B.15}$$

$$G_4^{04} = \begin{cases} \frac{\pi(2-8\varepsilon^6-7\varepsilon^2+8\varepsilon^4+2(3\varepsilon^2-3\varepsilon^4+\varepsilon^6-1)S)}{-\varepsilon^4 S^7} \\ \quad \text{with } S = \sqrt{1-\varepsilon^2}, \text{ if } 0<\varepsilon<1, \\ \frac{3}{4}\pi \quad \text{if } \varepsilon = 0, \end{cases} \tag{B.16}$$

$$G_4^{20} = \begin{cases} \frac{\pi}{\sqrt{(1-\varepsilon^2)^5}} & \text{if } 0<\varepsilon<1, \\ \pi & \text{if } \varepsilon = 0, \end{cases} \tag{B.17}$$

$$G_4^{21} = \begin{cases} \frac{\pi\varepsilon}{\sqrt{(1-\varepsilon^2)^5}} & \text{if } 0<\varepsilon<1, \\ 0 & \text{if } \varepsilon = 0, \end{cases} \tag{B.18}$$

$$G_4^{22} = \begin{cases} \frac{-\pi(5\varepsilon^2-2-4\varepsilon^4+2\sqrt{(1-\varepsilon^2)^5})}{\varepsilon^4\sqrt{(1-\varepsilon^2)^5}} \\ \text{if } 0<\varepsilon<1, \\ \frac{1}{4}\pi \quad \text{if } \varepsilon = 0. \end{cases} \tag{B.19}$$

Appendix C. Nomenclature

$C(t)$	integration "constant"
C^{st}	structural damping per unit length
$\overline{d}_n$	reduced modal damping $\overline{d}_n = -\sigma_n/\omega^{st}$
f, f_r, f_s	flow/wall friction coefficients
f^{st}	structural frequency in vacuo
f_X, f_Y, f_C	nonlinear fluidelastic forces per unit length
f_X^{st}, f_Y^{st}	structural forces per unit length

$h(\theta, t)$	local gap
h_0, h_1	steady and fluctuating local gap
H	average annular gap
K^{st}	structural stiffness per unit length
L	rotor length
M_a	added mass of the fluid per unit length, $M_a = \pi\rho R^2/\delta$
M^{st}	modal mass of the rotor per unit length in vacuo
$p(\theta, t)$	gap averaged pressure
p_0, p_1	steady and fluctuating gap averaged pressure
R	rotor radius
$Q(t)$	flow rate
t	time
$u(\theta, t)$	tangential flow velocity
u_0, u_1	steady and fluctuating tangential flow velocity
$X(t), Y(t)$	rotor motion
X_0, Y_0	steady rotor position
γ	mass ratio, $\gamma = M_a/M^{st}$
δ	reduced gap: H/R
ε	reduced initial static eccentricity, $\varepsilon = X_0/H$
λ_n	eigenvalue of the flow-structure system
θ	azimuthal angle
ν_n	imaginary part of the eigenvalue λ_n
ρ	fluid density
σ_n	real part of the eigenvalue λ_n
τ_r, τ_s	shear stresses at the rotor and stator walls
ω_n	circular frequency
ϖ_n	reduced modal frequency, $\varpi_n = \nu_n/\omega^{st}$
ω^{st}	structural circular frequency in vacuo
ϕ	delay
Ω	spinning velocity
$\overline{\Omega}$	reduced rotor velocity $\overline{\Omega} = \Omega/\omega^{st}$

References

Antunes, J., Piteau, P., 2001. A nonlinear model for squeeze-film dynamics under axial flow. Proceedings of the 2001 ASME Pressure Vessels and Piping Conference, Atlanta, Georgia, USA, 22–26 July 2001, PVP-Vol. 420–2, pp. 53–62.

Antunes, J., Axisa, F., Grunenwald, T., 1996. Dynamics of rotors immersed in eccentric annular flow: Part 1—theory. Journal of Fluids and Structures 10, 893–918.

Antunes, J., Mendes, J., Moreira, M., Grunenwald, T., 1999. A theoretical model for nonlinear planar motions of rotors under fluid confinement. Journal of Fluids and Structures 13, 103–126.

Carpenter, P.W., Garrad, A.D., 1986. The hydrodynamic stability of flow over Kramer-type compliant surfaces. Part 2. Flow-induced surface instabilities. Journal of Fluid Mechanics 170, 199–232.

Genta, G., 1995. Vibrations of Structures and Machines—Practical Aspects. Springer, New York.

Ginsberg, J.H., 2001. Mechanical and Structural Vibrations. Wiley, New York.

Grunenwald, T., Axisa, F., Bennett, G., Antunes, J., 1996. Dynamics of rotors immersed in eccentric annular flow: Part 2—experiments. Journal of Fluids and Structures 10, 919–944.

Inada, F., Hayama, S., 2000. Mechanism of leakage-flow-induced vibrations—single-degree-of-freedom and continuous systems, Proceedings of the Seventh International Conference on Flow-Induced Vibration, FIV2000, Lucerne, Switzerland, 19–22 June 2000, pp. 811–818.

Kaneko, S., Tanaka, S., Watanabe, T., 2000. Leakage flow induced flutter of highly flexible structures, Proceedings of the Seventh International Conference on Flow-Induced Vibration, FIV2000, Lucerne, Switzerland, 19–22 June 2000, pp. 811–818.

Krämer, E., 1993. Dynamics of Rotors and Foundations. Spriger, New York.

Moreira, M., Antunes, J., Pina, H., 2000a. A theoretical model for nonlinear orbital motions of rotors under fluid confinement. Journal of Fluids and Structures 14, 635–668.

Moreira, Tissot, A., Antunes, J., 2000b. Experimental validation of theoretical models for the linear and nonlinear vibrations of immersed rotors. Proceedings of the Eighth International Symposium on Transport Phenomena and Dynamic of Rotating Machinery, ISROMAC-8, Honolulu, Hawaii, March 26–30, 2000, II, pp. 857–865.

Porcher, M.G., 1994. Contribution à l'Étude des Instabilités Fluide-Élastiques de Structures Tubulaires, sous Ecoulemen Axial Confiné. Ph.D. Thesis, Presented at University of Paris 6.

Porcher, M.G., 2000. Influence of the boundary conditions in a friction based model of fluid-elastic instability in axial flow. Proceedings of the Seventh International Conference on Flow-Induced Vibration, FIV2000, Lucerne, Switzerland, 19–22 June 2000, pp. 371–378.